ACS Catalysis

Research Article

pubs.acs.org/acscatalysis

Role of the Morphology and Surface Planes on the Catalytic Activity of Spinel $LiMn_{1.5}Ni_{0.5}O_4$ for Oxygen Evolution Reaction

Thandavarayan Maiyalagan, Katharine R. Chemelewski, and Arumugam Manthiram*

Electrochemical Energy Laboratory & Materials Science and Engineering Program The University of Texas at Austin, Austin, Texas 78712, United States

ABSTRACT: The electrocatalytic activity of the spinel oxide $LiMn_{1.5}Ni_{0.5}O_4$ with different morphologies (cubic, spherical, octahedral, and truncated octahedral) has been investigated for the oxygen evolution reaction (OER) in alkaline solutions that is of interest for metal−air batteries. The OER activity increases in the order truncated octahedral < cubic < spherical < octahedral, despite a larger surface area (2.9 $m^2\ g^{-1}$) for the spherical sample compared to nearly similar surface areas (0.3−0.7 $m^2\ g^{-1}$) for the other three samples. The high activity of the octahedral sample is attributed to the regular octahedral shape with low-energy {111} surface planes, whereas the lowest activity of the truncated octahedral sample is attributed to the high-energy {001} surface planes. The octahedral sample also exhibits the lowest Tafel slope of 70 mV dec^{-1} with the highest durability whereas the truncated octahedral sample exhibits the highest Tafel slope of 120 mV dec^{-1} with durability similar to the cubic and spherical samples. The study demonstrates that the catalytic activities of oxide catalysts could be tuned and optimized by controlling the surface morphologies/planes via novel synthesis approaches.

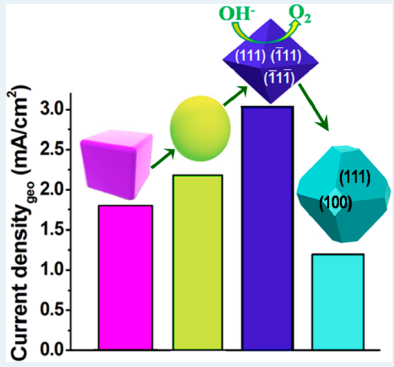

KEYWORDS: *oxygen evolution reaction, electrocatalysis, spinel oxides, nanostructures, crystal-plane effect, morphological effect*

1. INTRODUCTION

The oxygen evolution reaction (OER) plays a major role in several electrochemical devices, such as rechargeable metal−air batteries, water electrolyzers, electrosynthesis reactors, and metal electrowinning processes.[1−3] IrO_2 is the most widely investigated OER electrocatalyst due to its high catalytic activity and stability. However, iridium is expensive; so much effort has been devoted to develop alternate, less expensive OER catalysts with low overpotential.[4−6] Spinel oxides are a promising class of non-noble metal electrocatalysts for OER.[7−15]

Several factors, such as chemical composition, electronic structure, and surface atomic arrangement can influence the OER activity. For example, alloying of Pt and Pd has been shown to improve the catalytic activity for the oxygen reduction reaction (ORR).[16−20]Also, the catalytic activity of Pt and Pd for ORR is known to depend strongly on the surface planes, e.g., {100}, {110}, and {111} planes.[21,22] For example, Markovic et al.[23] reported the {111} planes of Pt to exhibit the highest activity for ORR. Also, the (111) facet of single crystal Pt_3Ni has been reported to exhibit orders of magnitude higher ORR activity than the conventional Pt/C catalysts,[24] and the high-index facets of Pt particles in size of 100−200 nm have been reported to exhibit the highest electrocatalytic activity that has ever been detected.[25]

However, despite extensive literature on the influence of composition, synthesis conditions, and size dependence[26,27] of spinel oxides on the OER activity, little information is available on the dependence of OER activity on the morphology and surface planes of spinel oxide electrocatalysts.[28] The lack of such information is partly due to the difficulty of stabilizing the various surface planes in oxides while maintaining good compositional control. We present here, for the first time, a systematic investigation of the influence of the morphology and surface planes/facets of the spinel oxides on OER by taking $LiMn_{1.5}Ni_{0.5}O_4$ spinel as an example. The $LiMn_{1.5}Ni_{0.5}O_4$ spinel with various morphologies and surface planes, e.g., octahedral, truncated octahedral, spherical, and cubic morphologies, are obtained by controlled synthesis processes, characterized by X-ray diffraction and scanning electron microscopy, and evaluated for OER.

2. EXPERIMENTAL SECTION

2.1. Synthesis. The precursors for the octahedral and spherical morphologies were prepared with a tank reactor by coprecipitating, respectively, the hydroxides and carbonates of Mn and Ni with sodium hydroxide and sodium carbonate and employing ammonium hydroxide as a complexing agent.[29] The pH value was kept at 10 and 8, respectively, for the hydroxide and carbonate precursors. The hydroxide precursor for the truncated octahedral sample was prepared by the coprecipitation method of mixing a solution containing the required quantities of manganese acetate and nickel acetate with KOH. The precursors for the cubic samples were synthesized by a hydrothermal method.[29,30] For the cubic precursor, urea and cetyl trimethylammonium bromide (CTMB) surfactant were mixed with stoichiometric amounts of $MnCl_2$ and $NiCl_2$ in

Received: October 26, 2013
Revised: December 17, 2013
Published: December 23, 2013

deionized water and heated at 150 °C for 15 h in a PTFE-lined autoclave. All the hydroxide, carbonate, chloride, and sulfate precursors were collected by rinsing with deionized water, followed by firing the oven-dried hydroxide precursors with a required amount of $LiOH{\cdot}H_2O$ at 900 °C in air for 15 h to produce the final spinel samples.

2.2. Structural and Morphological Characterization. The stoichiometric compositions of the synthesized spinel samples were verified by a Varian 715-ES inductively coupled plasma-atomic emission spectrometer (ICP-AES). The crystal structure of the sample was analyzed by X-ray diffraction (XRD) with a Rigaku Ultima-IV X-ray diffractometer and Cu Kα radiation in the 2θ range of 10−80° at an interval of 0.02° system. The morphology and particle size were obtained with scanning electron microscopy (Hitachi S-5500 SEM equipped with STEM) operated at 20 KeV. Multipoint Brunauer−Emmett−Teller (BET) surface area data were collected with an automatic nitrogen gas absorption analyzer (NOVA 2000, Quantachrome) using physical adsorption at 77 K.

2.3. Electrochemical Characterization. A commercial glassy carbon (GC) rotating disk electrode (RDE) (PINE, 5 mm diameter, 0.196 cm^2) was polished to a mirror-like finish and thoroughly cleaned. The preparation of the working electrode was performed as described below: ethanol suspensions containing 16 mg of catalyst per mL and 0.02 wt % Nafion (diluted from 5 wt % solution, EW1000, Dupont) were obtained by ultrasonic mixing for about 20 min. The 24.5 μL of the catalyst ink suspension thus obtained was coated onto the polished GC electrode. Electrochemical studies were carried out with a standard three-electrode cell connected to an Autolab electrochemical working station. Pt gauze was used as the counter electrode, saturated calomel electrode (SCE) was used as the reference electrode, and the spinel-coated GC was used as the working electrode. The measured potential, however, was converted in reference to reversible hydrogen electrode (RHE). Electrochemical activities of the catalysts were assessed by linear sweep voltammetry (LSV) and Tafel plots. LSV was performed in 0.1 M KOH (pH = 13) electrolyte with a scan rate of 20 mV s^{-1}. Tafel plots were recorded at a scan rate of 1 mV s^{-1}. All the electrochemical experiments were carried out in an oxygen atmosphere.

3. RESULTS AND DISCUSSION

The X-ray diffraction (XRD) data presented in Figure 1 confirm the formation of the cubic spinel ($Fd3m$) phase for all the four morphologies: cubic, spherical, octahedral, and truncated octahedral. The diffraction peaks at 18.82°, 36.34°, 44.20°, and 64.36° correspond, respectively, to the (111), (311), (400), and (440) planes of spinel $LiMn_{1.5}Ni_{0.5}O_4$ (JCPDS 32-0581). The implication of this impurity phase is an increase in the Mn/Ni ratio in the spinel phase and a consequent reduction of a small amount of Mn^{4+} to Mn^{3+} to maintain charge neutrality.

Figure 2 shows the SEM images of the four morphologies. The particle size of the cubic and spherical samples is larger than that of the octahedral and truncated octahedral samples. The cubic sample is about 10−20 μm in size with a mixture of {111} and {112} surface planes, as was reported in our previous investigation.[29] The spherical sample is about 10 μm in size but is composed of numerous nanoscale octahedral crystals as reported by us before.[29] The octahedral sample is 1 μm in size, with regular octahedral shape and {111} surface planes. The truncated octahedral sample is about 1 μm in size with {111}

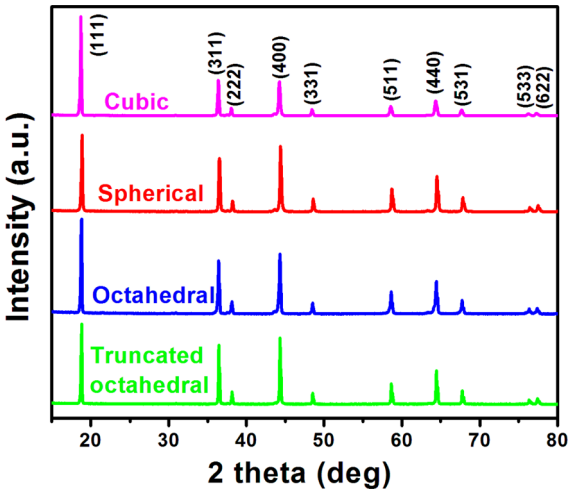

Figure 1. XRD patterns of the $LiMn_{1.5}Ni_{0.5}O_4$ samples.

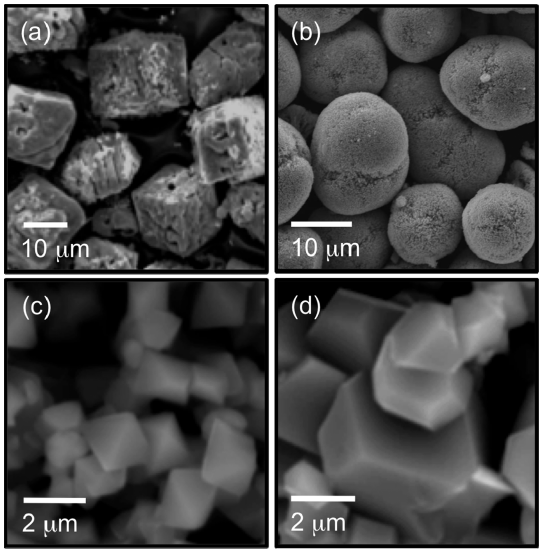

Figure 2. FE-SEM images of the $LiMn_{1.5}Ni_{0.5}O_4$ samples with various morphologies: (a) cubic, (b) spherical, (c) octahedral, and (d) truncated octahedral.

planes and truncated {001} planes. Schematic drawings depicting the various morphologies and crystallographic planes are shown in Figure 3. The truncated and octahedral particles are composed of smooth, single-crystal surface planes. The cubic sample has two predominant crystal planes, with some surface irregularity and roughness. The spherical particles have some single-crystal octahedral particle surfaces but with variations and imperfections. Detailed characterization of the crystal planes along with the TEM evidence can be seen in our earlier investigations.[29,30]

The electrocatalytic activity of the four samples for OER was evaluated in alkaline solutions by LSV in oxygen saturated 0.1 M KOH solution at a scan rate of 20 mV s^{-1}.The apparent current densities vs potential curves were normalized to the geometric area of the substrate, without any correction for ohmic drop, and the results are presented in Figure 3. A histogram comparing the activities of the four samples is given in Figure 4. Despite the same chemical composition and final synthesis temperature, the four morphologies exhibit marked differences in their OER activities. The OER activity increases

dx.doi.org/10.1021/cs400981d | ACS Catal. 2014, 4, 421−425

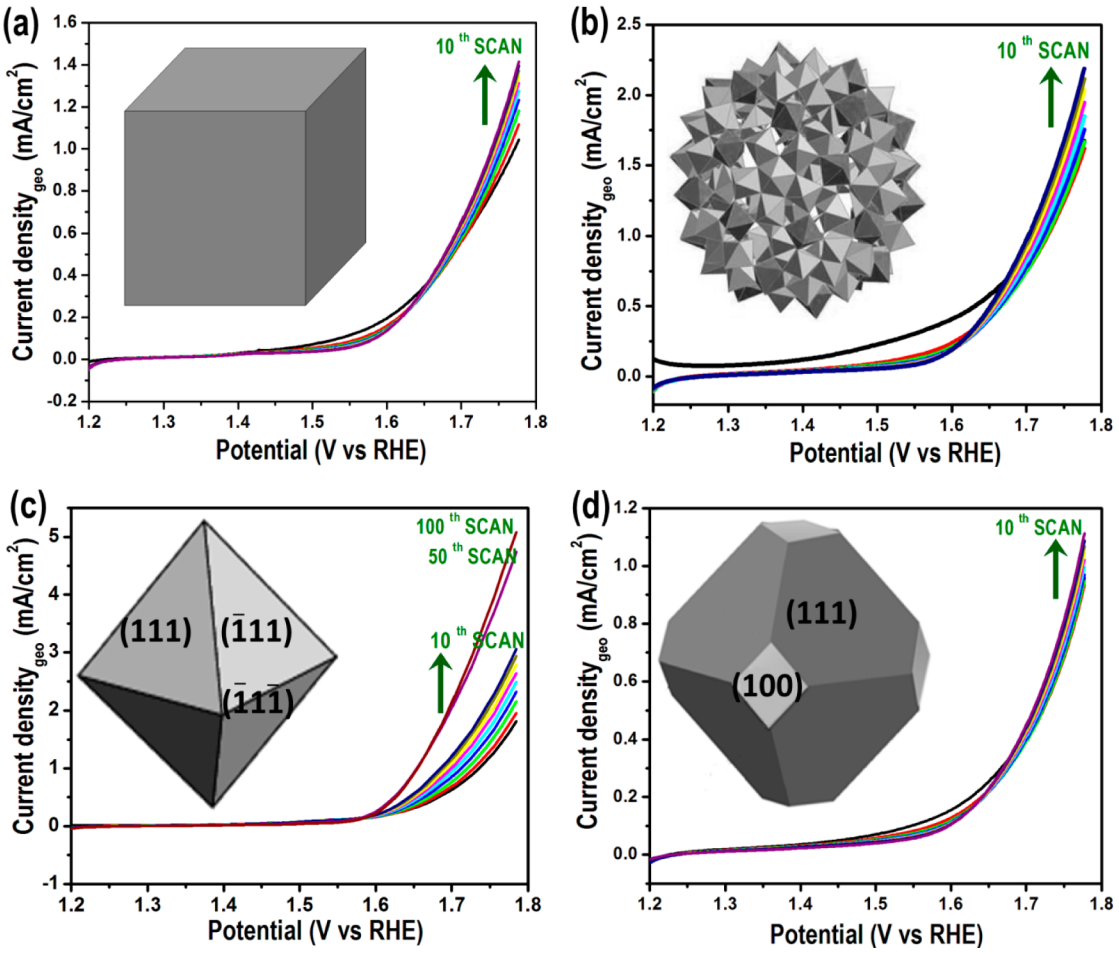

Figure 3. Linear sweep voltammograms of the $LiMn_{1.5}Ni_{0.5}O_4$ samples in 0.1 M KOH at a scan rate of 20 mV s^{-1}: (a) cubic, (b) spherical, (c) octahedral, and (d) truncated octahedral.

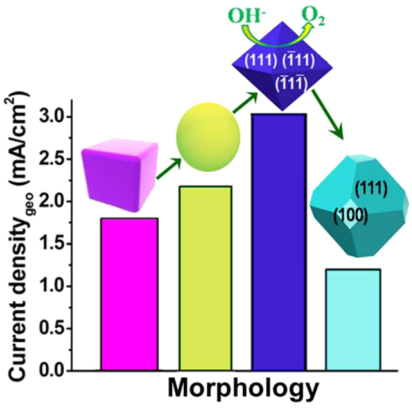

Figure 4. Histogram illustrating the shape-dependent electrocatalytic activity of $LiMn_{1.5}Ni_{0.5}O_4$ spinel oxides for OER.

in the order truncated octahedral < cubic < spherical < octahedral. For example, the specific catalytic activities of the truncated octahedral, cubic, spherical, and octahedral samples are, respectively, 1.1, 1.7, 2.2, and 3.3 mA/cm^2 at 1.7 V vs RHE. Clearly, the octahedral sample with all {111} surface planes exhibit superior activity compared to the other samples, whereas the truncated octahedral sample with truncated {001} planes exhibit the lowest activity. The octahedral sample also exhibits a ∼ 2-fold enhancement in the current density measured at 1.78 V at the 10th cycle and an ∼3-fold enhancement at the 100th cycle relative to the 1st cycle. The spherical sample shows higher activity than the cubic sample as it is composed of nanoscale octahedral crystals. Although the cubic, octahedral, and truncated octahedral samples exhibit similar surface areas of, respectively, 0.3, 0.7, and 0.3 m^2 g^{-1}, the spherical sample exhibits a larger surface area of 2.9 m^2 g^{-1} because it is composed of a smaller secondary particle (∼300 nm). Despite a significantly larger surface area, the spherical sample shows lower activity than the octahedral sample. This clearly demonstrates that the morphology and surface planes play a dominant role in controlling the OER activity. Computational calculations have shown that the {001} planes have a higher energy than the {111} planes;[31] obviously, the lower energy of the {111} planes in the octahedral sample is manifested in higher catalytic activity.

To gain further support, the electrochemical kinetics (Tafel plot) of the four samples was assessed and the data are presented in Figure 5. The Tafel slopes for the cubic, spherical, octahedral, and truncated octahedral samples are, respectively, 120, 73, 70, and 92 mV dec^{-1}. The octahedral and spherical morphologies exhibit a Tafel slope of 70 mV dec^{-1}, which is consistent with the values of 60−80 mV dec^{-1} observed for OER in alkaline or neutral electrolytes.[32−38] For example, Co_3O_4 nanocrystals on graphene and PbO_2 have been reported to exhibit a similar Tafel slope of, respectively, 67 and 70 mV dec^{-1}.[37] A value of 59 mV dec^{-1} observed for cobalt phosphate (Co−Pi) in neutral electrolyte corresponds to 2.3 × *RT*/*F*,

dx.doi.org/10.1021/cs400981d | *ACS Catal.* 2014, 4, 421−425

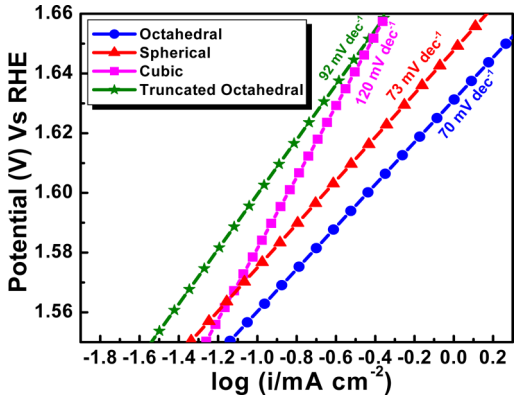

Figure 5. Tafel plots of the various morphologies of $LiMn_{1.5}Ni_{0.5}O_4$ spinel oxides for OER.

which is characteristic of an OER involving a reversible one-electron transfer prior to a chemical turnover-limiting step.[34] The unusually high Tafel slope of 120 mV dec^{-1} exhibited by the cubic sample implies a sluggish OER. Similar higher Tafel slopes of ~120 mV/decade have been reported for bulk $LiCoO_2$ and $LiCoPO_4$ particles without any particular morphology.[36,39]

The durability of the catalysts was assessed by chronoamperometric measurements at 25 °C, and the data are shown in Figure 6. The data were collected at a potential of 1.7 V for a

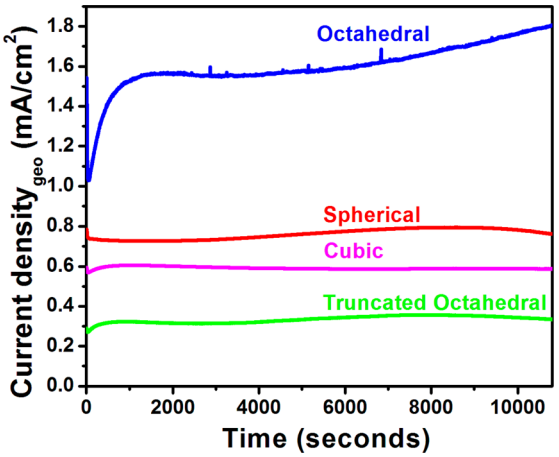

Figure 6. Polarization current vs time plots of the $LiMn_{1.5}Ni_{0.5}O_4$ spinel oxide with various morphologies at 1.7 V in 0.1 M KOH solution: (a) octahedral, (b) spherical, (c) cubic, and (d) truncated octahedral.

period of 3 h. The current density remains nearly constant throughout the test for the cubic, spherical, and truncated octahedral samples during the 3 h test. In contrast, the octahedral sample exhibits rather an increase in current density with time, illustrating a remarkable stability. Thus, the durability is also controlled by the surface planes similar to the OER activity, with the octahedral morphology with {111} surface planes exhibiting better stability. The better stability of the octahedral crystal is consistent with the lower energy of the {111} planes compared to the {001} planes.[40]

4. CONCLUSION

With an aim to understand the role of morphology and surface planes on OER activity, the $LiMn_{1.5}Ni_{0.5}O_4$ spinel in four different morphologies (cubic, spherical, octahedral, and truncated octahedral) has been systematically investigated. The octahedral sample with the {111} surface planes exhibits the highest OER activity with the best stability due to the low surface-energy planes. On the other hand, the truncated octahedral sample with truncated high-energy {001} planes exhibits the lowest OER activity. Although the dependence of ORR activity on surface planes has been well documented with metal electrocatalysts such as Pt or Pd, such studies are lacking with oxide OER catalysts partly due to the difficulty in realizing specific morphologies or surface planes with oxides. This study initiates such an activity through controlled synthesis, and a systematic investigation with various other oxide electrocatalysts could lead to potentially viable low-cost ORR and OER electrocatalysts for metal–air batteries.

AUTHOR INFORMATION

Corresponding Author

*A. Manthiram. Phone: (512) 471-1791. Fax: 512-471-7681. E-mail: manth@austin.utexas.edu.

Notes

The authors declare no competing financial interest.

ACKNOWLEDGMENTS

This work was supported by the U.S. Department of Energy, Office of Basic Energy Sciences, Division of Materials Sciences and Engineering under award number DE-SC0005397.

REFERENCES

(1) Trasatti, M. *J. Electroanal. Chem.* **1980**, *111*, 125–131.
(2) Rossmeisl, J.; Qu, Z.-W.; Zhu, H.; Kroes, G.-J.; Nørskov, J. K. *J. Electroanal. Chem.* **2007**, *607*, 83–89.
(3) Divisek, J.; Malinowski, P.; Mergel, J.; Schmitz, H. *Int. J. Hydrogen Energy* **1988**, *13*, 141–150.
(4) Gordon, R. B.; Bertram, M.; Graedel, T. E. *Proc. Natl. Acad. Sci. U. S. A.* **2006**, *103*, 1209–1214.
(5) Minguzzi, A.; Alpuche-Aviles, M. A.; Rodríguez Lopez, J.; Rondinini; Bard, A. J. *Anal. Chem.* **2008**, *80*, 4055–4064.
(6) Miles, M. H. *J. Electroanal. Chem.* **1975**, *60*, 89–96.
(7) Felix, C.; Maiyalagan, T.; Pasupathi, S.; Bladergroen, B. J.; Linkov, V. *Int. J. Electrochem. Sci.* **2012**, *7*, 12064–12077.
(8) Rios, E.; Gautier, J. L.; Poillerat, G.; Chartier, P. *Electrochim. Acta* **1998**, *44*, 1491–1497.
(9) Cong, H. N.; Abbassi, K. E.; Chartier, P. *J. Electrochem. Soc.* **2002**, *149*, A525–A530.
(10) Marsan, B.; Fradette, N.; Beaudoin, G. *J. Electrochem. Soc.* **1992**, *137*, 1889–1896.
(11) Cheng, F.; Shen, J.; Peng, B.; Pan, Y.; Tao, Z.; Chen, J. *Nat. Chem.* **2011**, *3*, 79–84.
(12) Wang, L.; Zhao, X.; Lu, Y. H.; Xu, M. W.; Zhang, D. W.; Ruoff, R. S.; Stevenson, K. J.; Goodenough, J. B. *J. Electrochem. Soc.* **2011**, *158*, A1379–A1382.
(13) Goodenough, J. B. *Chem. Mater.* **2010**, *22*, 587–603.
(14) Lee, S. W.; Carlton, C.; Risch, M.; Surendranath, Y.; Chen, S.; Furutsuki, S.; Yamada, A.; Nocera, D. G.; Shao-Horn. *J. Am. Chem. Soc.* **2012**, *134*, 16959–16962.
(15) Rios, E.; Chen, Y.-Y.; Gracia, M.; Marco, J. F.; Gancedo, J. R.; Gautier, J. L. *Electrochim. Acta* **2001**, *47*, 559–566.
(16) Zhang, H.; Jin, M.; Xia, Y. *Chem. Soc. Rev.* **2012**, *41*, 8035–8049.
(17) Guo, S.; Zhang, S.; Sun, S. *Angew. Chem., Int. Ed.* **2013**, *52*, 8526–8544.
(18) Balbuena, P. B.; Callejas-Tovar, R.; Hirunsit, P.; Martínez De La Hoz, J. M.; Ma, Y.; Ramírez-Caballero, G. E. *Top. Catal.* **2012**, *55*, 322–325.
(19) Xiao, J.; Kuang, S.; Yang, Q.; Xiao, F.; Wang, S.; Guo, L. *Sci. Rep.* **2013**, *3*, 2300–2304.

(20) Zhou, K.; Li, Y. *Angew. Chem., Int. Ed* **2013**, *51*, 602−613.
(21) Xie, S.; Choi, S. I.; Xia, X.; Xia, Y. *Curr. Opin. Chem. Eng.* **2013**, *2*, 142−150.
(22) Shao, M.; Yu, C.; Odell, J. H.; Jin, M.; Xia, Y. *Chem. Commun.* **2011**, *47*, 6566−6568.
(23) Gasteiger, H. A.; Markovic, N. M. *Science* **2009**, *324*, 48−49.
(24) Stamenkovic, V. R.; Fowler, B.; Mun, B. S.; Wang, G. F.; Ross, P. N.; Lucas, C. A.; Markovic, N. M. *Science* **2007**, *315*, 493−497.
(25) Tian, N.; Zhou, Z. Y.; Sun, S. G.; Ding, Y.; Wang, Z. L. *Science* **2007**, *316*, 732−735.
(26) Kwon, G.; Ferguson, G. A; Heard, C. J.; Tyo, E. C.; Yin, C.; Debartolo, J.; Seifert, S.; Winans, R. E.; Kropf, A. J.; Greeley, J.; Johnston, R. L.; Curtiss, L. A.; Pellin, M. J.; Vajda, S. *ACS Nano* **2013**, *7*, 5808−5817.
(27) Esswein, A.; McMurdo, J.; Ross, P. N.; Bell, A. T.; Tilley, T. D. *J. Phys. Chem. C* **2009**, *113*, 15068−15072.
(28) Hamdani, M.; Singh, R. N.; Chartier, P. *Int. J. Electrochem. Sci.* **2010**, *5*, 556−577.
(29) Chemelewski, K. R.; Lee, E.-S.; Li, W.; Manthiram, A. *Chem. Mater.* **2013**, *25*, 2890−2897.
(30) Chemelewski, K. R.; Shin, D. W.; Li, W.; Manthiram, A. *J. Mater. Chem. A* **2013**, *1*, 3347−3354.
(31) Karim, A.; Fosse, S.; Persson, K. A. *Phys. Rev. B* **2013**, *87*, 075322−075326.
(32) Chi, B.; Li, J.; Han, Y.; Chen, Y. *Int. J. Hydrogen Energy* **2004**, *29*, 605−610.
(33) Castro, E. B.; Real, S. G.; Pinheiro, L. F. *Int. J. Hydrogen Energy* **2004**, *29*, 255−261.
(34) Kanan, M. W.; Nocera, D. G. *Science* **2008**, *321*, 1072−1075.
(35) Dincă, M.; Surendranath, Y.; Nocera, D. G. *Proc. Natl. Acad. Sci. U. S. A.* **2010**, *107*, 10337−10341.
(36) Surendranath, Y.; Kanan, M. W.; Nocera, D. G. *J. Am. Chem. Soc.* **2010**, *132*, 16501−16509.
(37) Liang, Y.; Li, Y.; Wang, H.; Zhou, J.; Wang, J.; Regier, T.; Dai, H. *Nat. Mater.* **2011**, *10*, 780−786.
(38) Miles, M. H.; Huang, Y. H.; Srinivasan, S. *J. Electrochem. Soc.* **1978**, *125*, 1931−1934.
(39) Tseung, A. C. C.; Jansen, S. *Electrochim. Acta* **1977**, *22*, 31−34.
(40) Zhou, Z. Y.; Tian, N.; Li, J. T.; Broadwell, L.; Sun, S. G. *Chem. Soc. Rev.* **2011**, *40*, 4167−4185.